Medical & Biological Engineering & Computing
https://doi.org/10.1007/s11517-024-03157-1

ORIGINAL ARTICLE

DNN-BP: a novel framework for cuffless blood pressure measurement from optimal PPG features using deep learning model

S. M. Taslim Uddin Raju[1] · Safin Ahmed Dipto[1] · Md Imran Hossain[1] · Md. Abu Shahid Chowdhury[2] · Fabliha Haque[1] · Ayesha Tun Nashrah[2] · Araf Nishan[3] · Md Mahamudul Hasan Khan[1] · M. M. A. Hashem[1]

Received: 5 June 2023 / Accepted: 10 June 2024

Abstract
Continuous blood pressure (BP) provides essential information for monitoring one's health condition. However, BP is currently monitored using uncomfortable cuff-based devices, which does not support continuous BP monitoring. This paper aims to introduce a blood pressure monitoring algorithm based on only photoplethysmography (PPG) signals using the deep neural network (DNN). The PPG signals are obtained from 125 unique subjects with 218 records and filtered using signal processing algorithms to reduce the effects of noise, such as baseline wandering, and motion artifacts. The proposed algorithm is based on pulse wave analysis of PPG signals, extracted various domain features from PPG signals, and mapped them to BP values. Four feature selection methods are applied and yielded four feature subsets. Therefore, an ensemble feature selection technique is proposed to obtain the optimal feature set based on major voting scores from four feature subsets. DNN models, along with the ensemble feature selection technique, outperformed in estimating the systolic blood pressure (SBP) and diastolic blood pressure (DBP) compared to previously reported approaches that rely only on the PPG signal. The coefficient of determination (R^2) and mean absolute error (MAE) of the proposed algorithm are 0.962 and 2.480 mmHg, respectively, for SBP and 0.955 and 1.499 mmHg, respectively, for DBP. The proposed approach meets the Advancement of Medical Instrumentation standard for SBP and DBP estimations. Additionally, according to the British Hypertension Society standard, the results attained Grade A for both SBP and DBP estimations. It concludes that BP can be estimated more accurately using the optimal feature set and DNN models. The proposed algorithm has the potential ability to facilitate mobile healthcare devices to monitor continuous BP.

Keywords Blood pressure · Photoplethysmogram · Feature extraction · Feature selection algorithm · Deep neural networks

1 Introduction

Hypertension or elevated blood pressure (BP) is a critical medical condition that significantly enhances the risks of developing brain, kidney, heart, and other diseases [1, 2]. Continuous BP measurement and monitoring the variations in BP are essential for regulating high BP and early intervention in hypertension and other cardiovascular disorders [3]. Sphygmomanometery and oscillometry are frequently used for monitoring BP at domicile and mobile [4, 5]. Inflatable cuffs are used to measure non-invasive BP, which can be uncomfortable, especially for hypertensive patients who need regular readings. Since stress or anxiety can arise in patients using the cuff-based approach, the measured BP results can be influenced by this [6]. As a result, cuff-based methods have been proven to be a hindrance to the widespread use of BP monitoring. Therefore, non-invasive and continuous methods for BP estimation are highly required for alleviating hypertension.

Recent advances in sensor technology have made it possible to monitor physiological parameters unobtrusively anywhere, anytime [7–9]. In this regard, photoplethysmogram (PPG) signal is crucial for the assessment of vital health-related factors without a reference signal and clinical condition [10]. PPG is a simple, low cost optical technique having the ability to detect the variations in blood volume in the microvascular bed of tissue with each cardiac cycle [9]. A typical two-pulse PPG signal with its characteristic points is

Extended author information available on the last page of the article

Published online: 04 July 2024

depicted in Fig. 1. PPG's simplicity, portability, and low cost enable its integration into mobile and wearable devices, giving an alternative for ubiquitous monitoring [7, 11]. However, despite these benefits, PPG technology's susceptible nature towards noise and motion artifacts caused by moving fingers or hands extends the space between the sensor and the user's skin and alters the signal quality [12]. This hinders the robust assessment of physiological parameters, making them impracticable for clinical applications [13].

In recent years, machine learning approaches have been used to attain excellent outcomes for continuous BP measurement using PPG signals. Recent researches have established the relation between the PPG signal and BP values [14–18]. Non-invasive BP estimation from PPG signals can be done by analyzing two PPG pulse waves or a PPG pulse wave along with an electrocardiogram wave [19]. Researches have been continued to explore methods of estimating BP using features of the PPG signal only. X. Teng and Y. Zhang in [20] utilized only the PPG signals to measure BP for the first time. N. Hasanzadeh et al. in [14] proposed a BP estimation method using PPG signal and its morphological features. M. H. Chowdhury et al. in [15] used 107 demographic features for estimating BP from the PPG signal. In addition, ReliefF feature selection (FS) method was applied to select optimal feature set. P. Li et al. in [21] developed a feed-forward neural network to estimate the BP using PPG features extracted by semi-classical signal analysis tools. Recently, deep neural networks have become the most widely used method because of their accurate results and cost-effective alternative to conventional machine learning methods [17, 21, 22]. A few BP estimation techniques from PPG signals are described in the literature, but most of them used only traditional machine learning methods and conventional feature selection techniques [23]. However, there were no specific feature selection algorithms to obtain the optimal feature set. Therefore, this paper aims to develop the deep learning approach along with an ensemble feature selection technique for the estimation of BP.

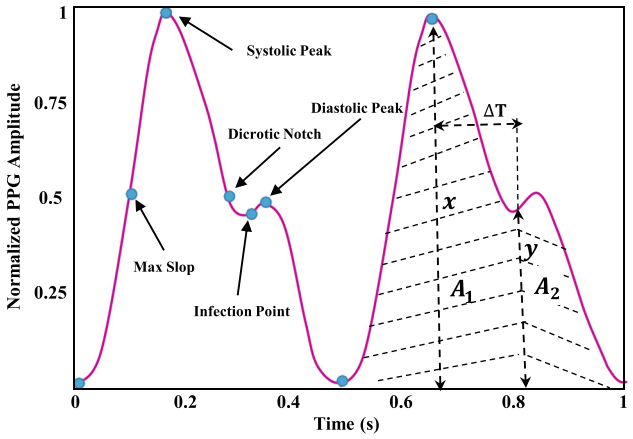

Fig. 1 A typical two-pulse PPG signal with its characteristic points. Here, x and y portrait the amplitudes of systolic and diastolic peaks, respectively, and ΔT is the time period between these two points. A_1/A_2 is the ratio of inflection

This paper proposes a cuff-less and continuous BP monitoring technique based on the characteristic features of the PPG signal and deep neural network. PPG signals are acquired from 219 subjects and checked the signal quality. Various preprocessing algorithms are applied to reduce noise and motion artifacts. After denoising, a total of 46 time and frequency domain features are extracted from the PPG signal, as well as its derivatives and first Fourier Transformed of PPG signal. An ensemble feature selection algorithm is applied to select the optimal feature set based on the voting of four FS techniques. Finally, DNN models are developed to estimate the SBP and DBP values. The major contributions of this paper are summarized as follows:

- Preprocessing the PPG signal, including the filtering, removing baseline wander (BW), and PPG wave normalization.
- Developing a peak detection algorithm and extracting a single PPG wave cycle having the highest positive systolic peak from the overall PPG waveform using it.
- Extracting the various domain features from preprocessed selected PPG cycle and its derivatives.
- Selecting the optimal features set through ensemble feature selection technique.
- Constructing DNN-based models with 10-fold cross-validation to estimate the SBP and DBP.

The sequence of the remaining sections of the paper is as follows: Section 2 describes the background details and motivation of the research. Section 3 describes the proposed methodology for cuff-less blood pressure estimation. Section 4 demonstrates feature selection results, the performance of proposed algorithm and its comparison with health standards and other works. Finally, Section 5 terminates the paper with future directions.

2 Background and related works

This section describes the recent studies that rely on only PPG signals to estimate BP. In the recent decade, many approaches for measuring cuff-less BP have been proposed as alternatives to traditional methods. M. Kachuee et al. [8] extracted

whole-based and physiological features and used the adaptive boosting algorithm (AdaBoost) to achieve a higher accuracy. One of the limitations of the proposed method is that the accuracy decreases due to lack of calibration. A. Gaurav et al. [24] extracted 8 PPG signal magnitude and temporal features and 19 more features from PPG's second derivative, called the acceleration plethysmogram waveform. These features were used to train and validate three artificial neural network (ANN) regression models for each DBP and SBP. However, the results for BP estimation were unsatisfactory because age and gender were not used as features. In another study, Y. Zhang and Z. Feng [16] applied a support vector machine (SVM) to predict BP, compared it with linear regression and ANN, and achieved better accuracy. Features were extracted from more than 7000 heartbeats and 9 parameters. However, the results for the estimation of BP were not good enough; mean error is 11.64 ± 8.20 mmHg for SBP and 7.617 ± 6.78 mmHg for DBP. S. S. Mousavi et al. [25] extracted whole-based features proposed by M. Kachuee et al. [8] and time or frequency domain features. N. Hasanzadeh et al. [14] presented a new algorithm for the robust detection of PPG key points and extracted some morphological key features. Therefore, the proposed method achieved a good correlation between the estimated BP and its actual value. The main drawback of their algorithm is that the accuracy of the algorithm decreases if the percentage of actual class members decreases.

A. Chakraborty et al. [7] introduced two distinct approaches for the estimation of SBP, MAP, and DBP, respectively. The first method used the Two-Pulse Synthesis (TPS) model based on the initialization method, while the second method used a learning based non-parametric regression technique for the measurement of BP. M. Panwar et al. [17] developed a model named PP-Net with a customized Long-term Recurrent Convolutional Network (LRCN), utilizing the convolutional neural network and long short-term memory for estimating the physiological parameters using a single channel PPG signal.

For each PPG signal, M. H. Chowdhury et al. [15] retrieved 107 features, including 65 time-domain, 16 frequency-domain, 10 statistical features along with 6 demographic data. The ReliefF feature selection method with gaussian process regression (GPR) showed promising results for introducing an accurate cuffless BP monitoring system. P. Li et al. [21] used the semi-classical signal analysis (SCSA) method to extract features from the PPG signal and compared the output results, and SVM with SCSA produced the overall highest accurate estimates among decision tree, multiple linear regression, and SVM. In addition, a single feed-forward neural network (FFNN) was utilized for BP estimation with PPG features, which are extracted by SCSA. S. Maqsood et al. [22] evaluated the performance of machine learning approaches, including traditional machine learning and deep learning. The experiment, which used the PPG-BP dataset and MIMIC-II database, demonstrated that time-domain characteristics performed better when deep learning methods were used. For SBP and DBP estimation, Gated Recurrent Units (GRU) and Bi-Directional Long Short-Term Memory (Bi-LSTM) provided the best results using time-domain features, respectively.

Table 1 represents several existing methods to estimate the blood pressure. Motivated by the advantages of PPG technology and shortcomings of the existing studies, we focus on developing an efficient deep learning framework with feature engineering for a better robust system. In addition, an ensemble feature selection technique is proposed to obtain the optimal features based on major voting scores.

3 Methodology

The overall architecture of the proposed cuff-less BP estimation algorithm is shown in Fig. 2. The main steps of the proposed method are as follows: (i) extracting the PPG signal as the primary input and checking the signal quality, (ii) applying the preprocessing algorithms on PPG signal for denoising and correcting the BW, (iii) extracting the characteristic wave features from preprocessed PPG signals, (iv) employing an ensemble feature selection strategy for selecting optimal feature set, (v) constructing DNN-based models with 10-fold cross-validation, and (vi) finally evaluating estimation accuracy of the models for SBP and DBP.

3.1 Basic principles

The fundamental principle of estimating BP with pulse transit time (PTT) is based on evaluating the velocity of pulse wave (PW) from its traveling time between two specific sections of the traveling path. The overall concept of pulse wave propagation through an artery can be modeled by propagating a pressure wave interior an elastic cylindrical tube with mechanical properties similar to arterial walls to correlate wall elasticity to PTT. The elasticity of an artery and the velocity of the pulse waves propagating through it are profoundly related. At each ventricular contraction, blood is ejected from the lower chambers of the heart to the arterial system by affecting the velocity of the blood, resulting in a pressure wave that travels along the elastic arteries [26]. It has been shown that elastic modulus (E) of the tube is related to the fluid pressure (P) for central arteries in an exponential

Table 1 Brief summary of the related works

Authors	Dataset	Techniques	Weakness/remarks
M. Kachuee et al. (2016) [8]	MIMIC II database (1000 subjects)	DWT, PCA, whole based and physiological feature extraction and regression algorithms (AdaBoost)	Cannot ensure higher accuracy for lack of calibration
A. Gaurav et al. (2016) [24]	MIMIC II database (3000 subjects)	Feature extraction and ANN	Can improve accuracy with inclusion of age and gender information
Y. Zhang and Z. Feng (2017) [16]	University of Queensland Vital Signs Database (19 subjects)	Feature extraction and SVM	Cannot perform well for shortage of data
S. S. Mousavi et al. (2018) [25]	MIMIC II database (441 subjects)	FFT, FFT^{-1}, Feature extraction, PCA and regression algorithms (AdaBoost)	Did not include data of healthy people for training proposed model
N. Hasanzadeh et al. (2019) [14]	MIMIC II (942 subjects)	Type I Chebyshev low-pass, morphological features extraction, regression algorithms (AdaBoost)	Did not include more low or high BP dataset and results affected due to variations in recording errors
A. Chakraborty et al. (2020) [7]	Own dataset (150 subjects)	Non-parametric regression technique	Can ensure better performance of model with more dataset
M. Panwar et al. (2020) [17]	MIMIC II database (1557 subjects)	LRCN deep learning algorithm	Need to include wide range of patients such as children, people lacking fine motor skills
M. H. Chowdhury et al. (2020) [15]	PPG-BP (222 recordings, 126 subjects)	Feature extraction, statistical, and demographic features, and GPR	Larger dataset fulfilling A grade requirement of BHS standard could be used
P. Li et al. (2021) [21]	MIMIC II database (8000 subjects)	SCSA feature extraction tool, FFNN	Can ensure effectiveness of model with larger dataset including healthy people and different categories of BP
S. Maqsood et al. (2021) [22]	PPG-BP (657 recordings, 219 subjects)	Temporal, statistical and frequency features of PPG, PPG′ and PPG″, GRU and Bi-LSTM models	Cannot show high accuracy for error in more robust results

* *DWT*, discrete wavelet decomposition; *PCA*, principal components analysis; *FFT*, Fast Fourier Transform; FFT^{-1} = Inverse Fast Fourier Transform; PPG′, 1st derivative of PPG; PPG″, 2nd derivative of PPG

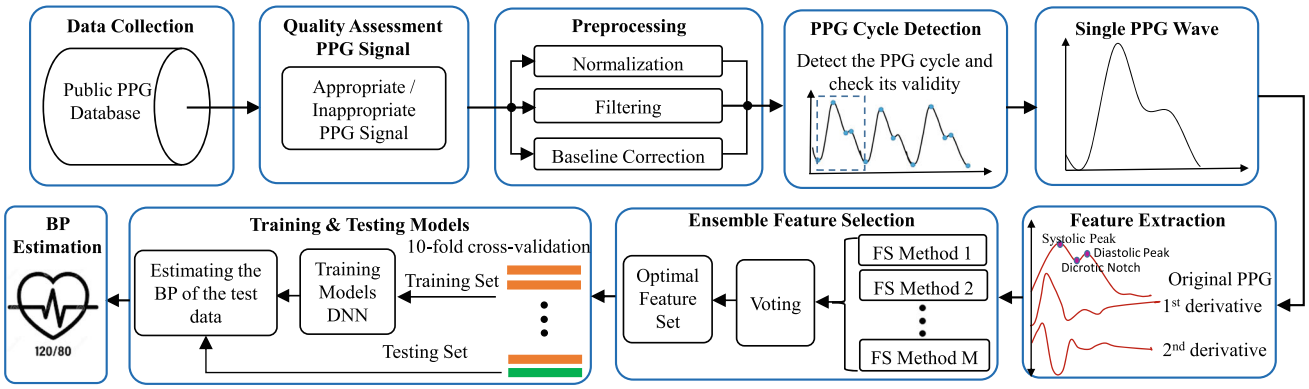

Fig. 2 Block diagram of the proposed blood pressure estimation algorithm

manner as

$$E = E_O.e^{\alpha.(P-P_O)} \tag{1}$$

where E_O is the elastic modulus at zero fluid pressure P_O and α is a correction factor.

The elasticity of the tube is described as far as Compliance (C), which is defined as the rate of change in cross-sectional area (A_m) of the tube with respect to pressure. C is determined by solving the conservation of mass and momentum equations, and it can be expressed as the function of P as in [8, 27]:

$$C(P) = \frac{A_m}{\pi P_1[1 + (\frac{P-P_0}{P_1})^2]} \tag{2}$$

where A_m, P_0, and P_1 vary from subject to subject.

Pressure wave propagating through a cylindrical shape elastic tube (see Chapter 3 of [28] for derivation) can be expressed mathematically as

$$P(x,t) = f(x \pm t/\sqrt{LC(P)}) \tag{3}$$

where x and t indicate space and time, respectively. According to this wave propagation equation, the velocity of pulse traveling along an artery, PWV, is $1/\sqrt{LC(P)}$, where $L = \rho/A$, in which ρ is the density of blood. Hence, PTT, the time interim for navigating the pulse wave through a tube of length k, is expressed as

$$PTT = K\sqrt{LC(P)} \tag{4}$$

Substituting the value of $C(P)$ and L, Eq. 4 can be rewritten as

$$PTT = K\sqrt{\frac{\rho A_m}{\pi A P_1[1 + (\frac{P-P_0}{P_1})^2]}} \tag{5}$$

where P is mean BP. Thus, it is elucidated from Eq. 5 that there exists an inverse relationship between PTT and BP. By Eq. 5, we can only estimate the mean BP with PTT based on arterial wave propagation model. However, DBP and SBP can also be estimated by new proposing indicator, PPG intensity ratio (PIR) [29] in terms of PTT. By solving the $M - K$ equation, we find that pulse pressure, PP, is inversely proportional to PTT^2 [30]. PP can be expressed in terms of PTT as

$$PP = PP_0(\frac{PTT_0}{PTT})^2 \tag{6}$$

where PP_0 and PTT_0 are initial calibrated values of PP and PTT, respectively. According to the two-element Windkessel model, as shown in [31], DBP is inversely proportional to the first power of PIR:

$$DBP \propto \frac{1}{PIR} \tag{7}$$

This indicates that DBP can easily be estimated from Eq. 7 with the aid of initially calibrated values of DBP and PIR are DBP_O and PIR_O, respectively.

$$DBP = DBP_0\frac{PIR_0}{PIR} \tag{8}$$

Since PP is the difference between SBP and DBP [32], so SBP can be derived from Eqs. 6 and 8 as

$$SBP = DBP_0\frac{PIR_0}{PIR} + PP_0(\frac{PTT_0}{PTT})^2 \tag{9}$$

3.2 Data description

In this paper, the online PPG-BP database was used as a source for the PPG signals [33]. Liang et al. [34] analyzed and evaluated the quality of these PPG signals. The authors developed a custom portable hardware system that consisted of a PPG sensor probe, a MSP430FG4618 microcontroller, and a specialized Android application for data management. The PPG sensor was equipped with dual LEDs with 660 nm (red light) and 905 nm (infrared) wavelengths, offering a high sampling rate of 1 kHz, a 12-bit analog-to-digital converter (ADC), and a bandpass hardware filter with a frequency range of 0.5 to 12 Hz. The MSP430FG4618 microcontroller was embedded on the probe to manage the ADC, collect data, and transmit it via Bluetooth to the app. Arterial blood pressure measurements were obtained using the Omron HEM-7201 upper arm monitor. The left index finger was used to collect fingertip PPG signal, and Omron HEM-720 was used for the

Table 2 Statistical patient details

Physical feature	Numerical data
Age (years)	57 ± 15
Gender	115 female (52%)
Height (cm)	161 ± 8
Weight (kg)	60 ± 11
SBP (mmHg)	127 ± 20
DBP (mmHg)	71 ± 11

* Note: all the numerical values are explained in mean $\pm$ standard deviation (range) and categorical values in frequency distribution (%)

collection of reference BP. The assessment of BP was carried out by a nurse within the hospital setting. Three PPG segments were collected from each subject during the BP recording. Therefore, the dataset consists of 657 recorded PPG signals from 219 subjects. The sampling rate of PPG signals was 1 kHz, and the duration of each signal was 2.1 s. Table 2 demonstrates the description of the basic physiological information and a concise statistical summary.

Several PPG signals in the dataset were noisy and unsuitable for feature extraction. The quality assurance process was applied to eliminate the unacceptable quality of the PPG signal by using the skewness quality index (SQI) [34]. The final dataset consists of 218 recorded signals associated with 125 unique subjects. Each recorded signal has its own unique ID. The unique ID is used in this study in order to prevent overlapping the subjects of the training set with the test set in

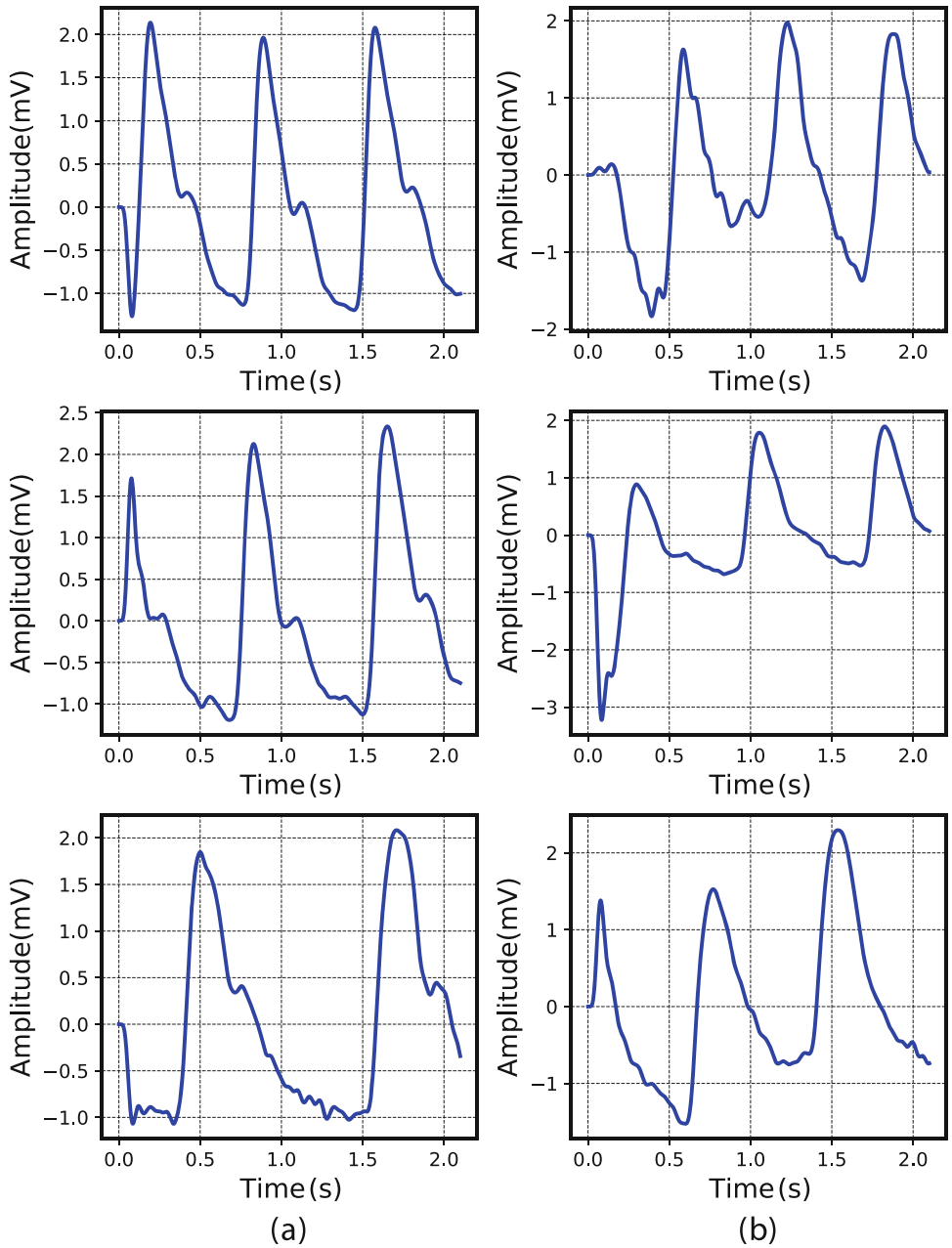

Fig. 3 Comparison of the PPG waveforms that are appropriate (fit) and inappropriate (unfit) in this study. **a** Appropriate PPG signal. **b** Inappropriate PPG signal

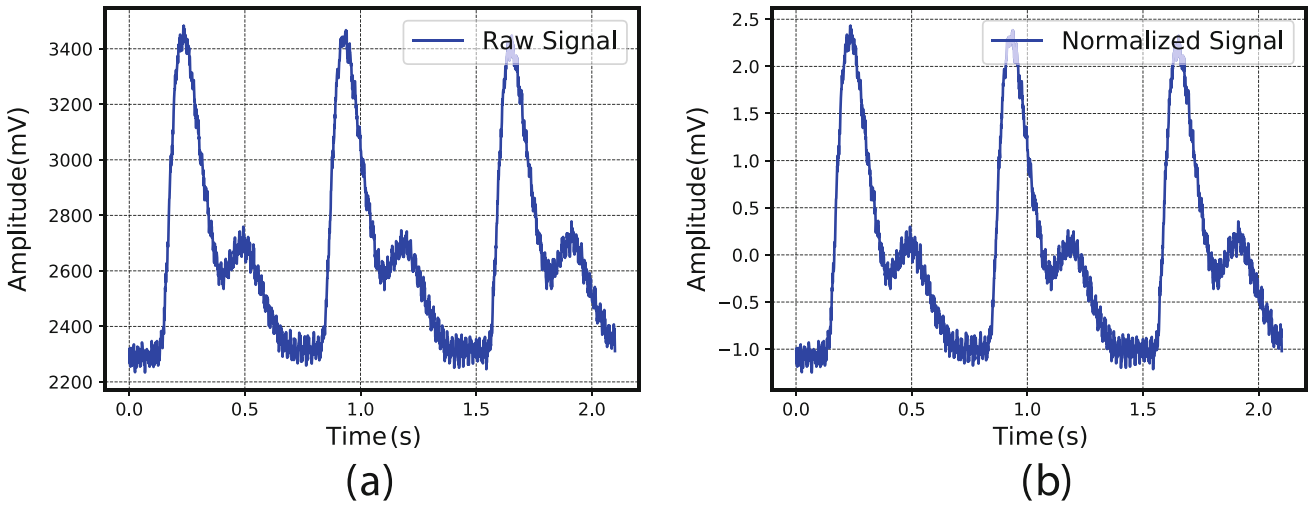

Fig. 4 PPG signal **a** before and **b** after normalization

DNN-based model. To evaluate the skewness quality index, the PPG signal was divided into two categories: appropriate and inappropriate, shown in Fig. 3. The fit waveforms have apparent systolic and diastolic features with dicrotic notches, and the unfit waveforms do not have dicrotic notch and other informative features.

3.3 Preprocessing signals

To get quality waveforms, various pre-processing approaches were used to eliminate the noise in the PPG signals [33]. After preprocessing, approximately 125 subjects were included for evaluation.

3.3.1 Normalization

Data normalization reduces data analysis complication. Through PPG signal normalization, the information within a database can be formatted in such a way that it can be visualized and analyzed. In this study, the PPG signal was normalized using the z-score method to get amplitude-limited data.

$$PPG_n = \frac{PPG_O - \mu(PPG_O)}{\sigma(PPG_O)} \tag{10}$$

where PPG_O represents the original PPG signal and PPG_n indicates normalized version of PPG_O. μ and σ denote the mean and standard deviation of the original PPG signal, respectively. Figure 4 shows the sample PPG signal before and after normalization.

3.3.2 Signal filtration

The raw PPG signal of the database [33] contains so many noise components. The primary purpose of filtering a signal is to smooth out and reduce high-frequency noise associated with measurement, such as power line interference, motion artifact, low amplitude of the PPG signal, etc. [35]. Firstly, filtering techniques were tested, such as 7th order low pass Butterworth filter [36], 9th order low pass cheby 1 filter, removing coverage FIR filter, Discrete Wavelet Transform (DWT) [37], and Fast Fourier Transform (FFT) [38].

Finally, low pass Butterworth filter is selected because, compared to the other methods, it was analyzed that low pass Butterworth filter provides several merits such as a better phase response, better visualization of systolic and diastolic peak, and more efficiency in terms of maximum noise reduction. Figure 5 shows that the 7th order low pass Butterworth filter with a cut-off frequency of 15 Hz produced the best noiseless signal which was designed in MATLAB.

3.3.3 Baseline correction

BW is a low-frequency artifact that occurs when a subject's PPG signal is recorded [39]. BW reduction is a critical step in the preprocessing of PPG signals because BW makes PPG recordings challenging to interpret. The primary source of BW in the PPG signal is the patient's movement and respiration [39]. Anything less than 0.5 Hz is a result of baseline wandering. In this study, baseline correction was done by fitting a 4th-degree polynomial to find the trend in the signal and then subtracted the trend to get the baseline-corrected signals, as shown in Fig. 6.

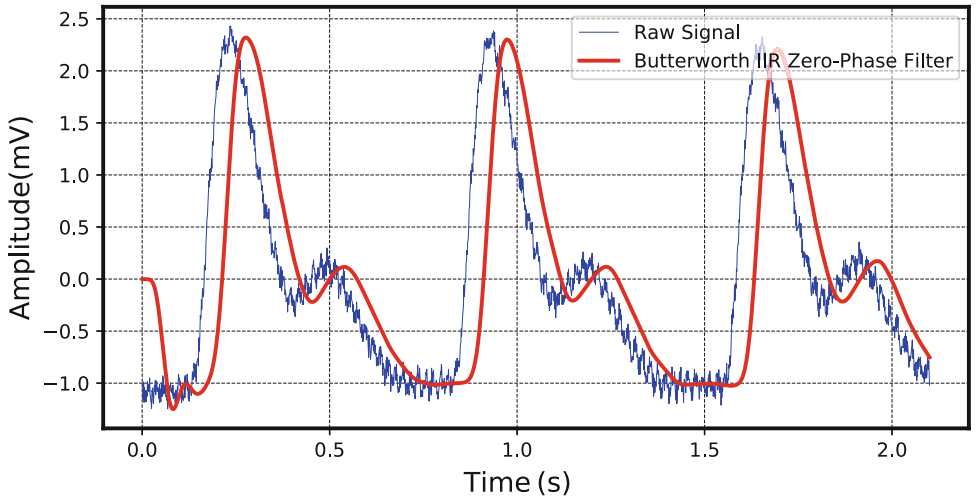

Fig. 5 Illustration of PPG signal before and after preprocessing. Filtered signal superimposed on the raw signal

3.4 Feature extraction

3.4.1 PPG cycle detection and selection

PPG signal is a continuous waveform, and every individual PPG cycle contains approximately the same information. In this study, one single PPG cycle was used to extract features. Therefore, PPG signals were segmented into a single cycle from 2.1s $time\_frame$ PPG signals representing a single heartbeat. Normally 2.1s 1 s $time\_frame$ PPG signals contain two or more cycles. A peak detection algorithm was used to locate the signal peaks. Then each PPG cycle C_{PPG} was stored in S_{PPG}. Then we extracted all valid PPG cycles. A C_{PPG} cycle is valid if it contained five important properties. Finally, the best one (B_{PPG}) was detected automatically by using the peak detection algorithm in Algorithm 1. The detected PPG cycle B_{PPG} in a S_{PPG} is depicted in Fig. 7.

Finally, by enhancing the analytical technique of Elgendi [35], 46 characteristic features are extracted from the B_{PPG}, as well as its derivatives (1st, and 2nd order), and Fast Fourier Transformed B_{PPG} signal. The distributions of these features are as follows: 21 (F_1 to F_{21}) from the B_{PPG} signal, 19 (F_{22}

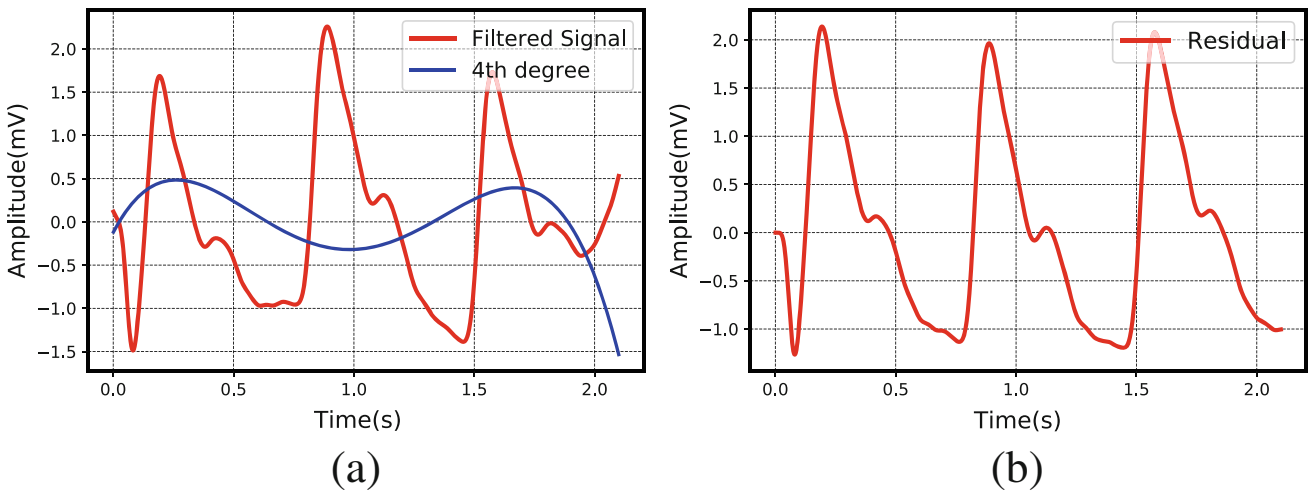

Fig. 6 Correction of the PPG signal's baseline, **a** PPG signal with baseline wandering and polynomial trend of fourth degree and **b** PPG signal after detrending

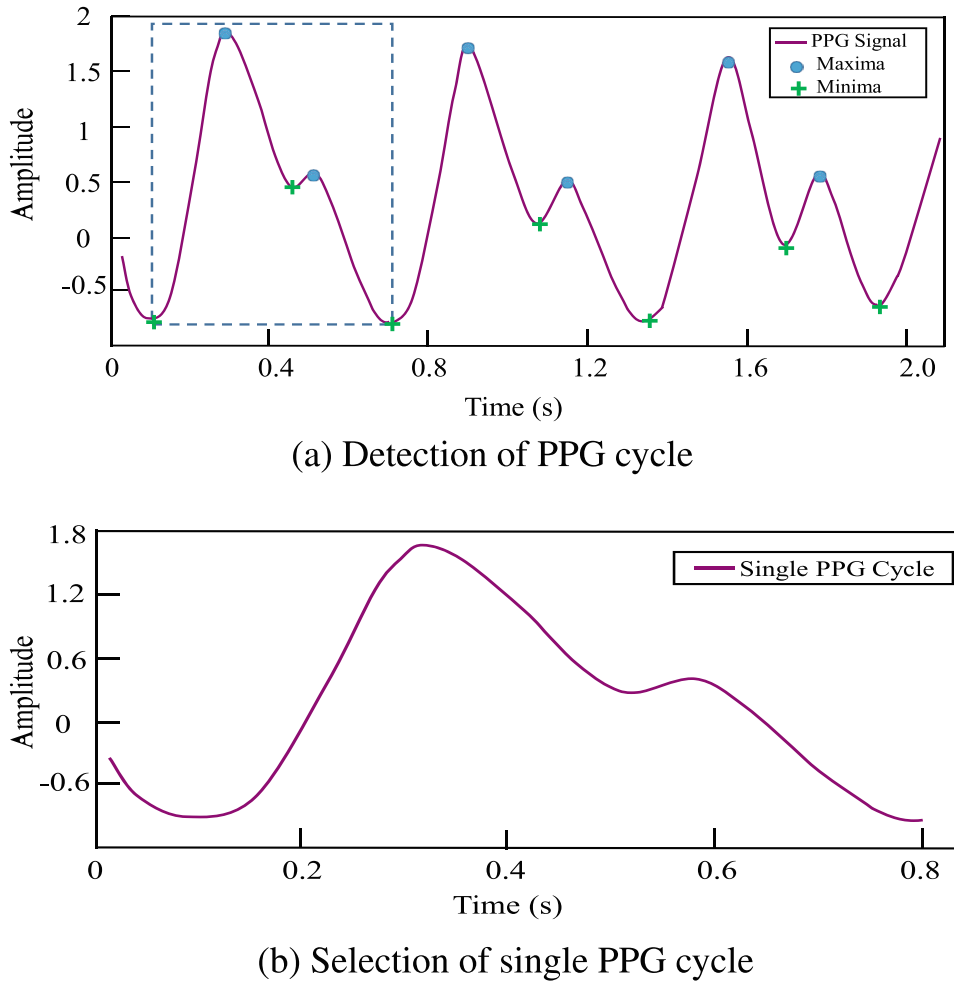

Fig. 7 Detection and selection of one single PPG cycle from continuous waveform of PPG signal

to F_{40}) from its derivatives (1st and 2nd order), and 6 (F_{41} to F_{46}) from the Fast Fourier Transformed B_{PPG} (Table 3). Additionally, age (F_{47}) and gender (F_{48}) are provided for each subject as features. Figure 8 depicts the characteristic features of the PPG signal.

3.5 Feature selection

Feature selection refers to selecting the most relevant and non-redundant features to be used in model construction. The fundamental objective of feature selection is to enhance the performance of a predictive model and minimize the computational cost of modeling by selecting the most effective features. Here, four feature selection methods are used: correlation-based feature selection (CFS), ReliefF feature selection (ReliefF), features for classification using minimum redundancy maximum relevance (FSCMRMR), and recursive feature elimination (RFE).

3.5.1 CFS

Correlation is a statistical approach that may be used to assess the presence and strength of relationships between pairs of features. An attribute is acceptable if relevant to the class but not redundant to any of the other relevant attributes [40]. Here, this paper uses the correlation coefficient probability ($p-value$) to make good feature subsets containing features highly correlated with the classification but uncorrelated.

3.5.2 ReliefF

ReliefF is a feature selection algorithm that takes a filtering approach for binary classification with discrete features [41]. This algorithm calculates a feature score for each feature applied to rank and thus chooses the top-scoring features. These scores can be considered as feature weights to handle downstream modeling. The ReliefF algorithm and its derivatives are the only individual evaluation filter algorithms

Table 3 Details of features extracted from each S_{PPG}

Features	Definition	Features	Definition
F_1: x	Systolic peak	F_2: y	Diastolic peak
F_3: z	Dicrotic notch	F_4: t_{p_i}	Pulse interval
F_5: y/x	Augmentation index	F_6: $(x-y)/x$	Alternative augmentation index
F_7: z/x	Ratio of dicrotic notch and systolic peak	F_8: $(y-x)/x$	Negative relative augmentation index
F_9: t_1	Systolic peak time	F_{10}: t_2	Dicrotic notch time
F_{11}: t_3	Diastolic peak time	F_{12}: $\Delta T = t_3 - t_1$	Systolic and diastolic peaks time difference
F_{13}: w	Full width at half systolic peak	F_{14}: $A_3/(A_1+A_2)$	Inflection poin area ratio (IPA)
F_{15}: $(A_2+A_3)/A_1$	Ratio of the area before and after dicrotic notch ($sVRI$)	F_{16}: t_1/x	Systolic peak rising slope
F_{17}: $y/(t_{pi}-t_3)$	Diastolic peak falling slope	F_{18}: t_1/t_{pi}	t_1 to t_{pi} ratio
F_{19}: t_2/t_{pi}	t_2 to t_{pi} ratio	F_{20}: t_3/t_{pi}	t_3 to t_{pi} ratio
F_{21}: $\Delta T/t_{pi}$	ΔT to t_{pi} ratio	F_{22}: t_{a_1}	Interval time from point l_1 to point a_1 for 1st derivative of PPG
F_{23}: t_{b_1}	Time interval from point l_1 to next point b_1	F_{24}: t_{e_1}	Interval time from point l_1 to point e_1
F_{25}: t_{l_1}	Time interval from point l_1 to next point l_1	F_{26}: t_{a_1}/t_{p_i}	a_1 (t_{a_1}) to t_{p_i} ratio
F_{27}: t_{b_1}/t_{p_i}	Ratio between time interval of b_1 (t_{b_1}) and pulse interval (t_{p_i})	F_{28}: t_{e_1}/t_{p_i}	Ratio between time interval of e_1 (t_{e_1}) and pulse interval (t_{p_i})
F_{29}: t_{l_1}/t_{p_i}	Ratio between time interval of l_1 (t_{l_1}) and pulse interval (t_{p_i})	F_{30}: b_2/a_2	Ratio of b_2 and a_2
F_{31}: e_2/a_2	Ratio of e_2 and a_2	F_{32}: $(b_2+e_2)/a_2$	Ratio of (b_2+e_2) and a_2
F_{33}: t_{a_2}	Time interval from point l_2 to next point a_2 of 2nd derivative PPG	F_{34}: t_{b_2}	Interval time from point l_2 to next point b_2
F_{35}: t_{a_2}/t_{p_i}	a_2 (t_{a_2}) to t_{p_i} ratio	F_{36}: t_{b_2}/t_{p_i}	b_2 (t_{b_2}) to t_{p_i} ratio
F_{37}: $(t_{a_1}+t_{a_2})/t_{p_i}$	Ratio of $(t_{a_1}+t_{a_2})$ and pulse interval (t_{p_i})	F_{38}: $(t_{b_1}+t_{b_2})/t_{p_i}$	Ratio of $(t_{b_1}+t_{b_2})$ and pulse interval (t_{p_i})
F_{39}: $(t_{e_1}+t_2)/t_{p_i}$	Ratio of $(t_{e_1}+t_2)$ and pulse interval (t_{p_i})	F_{40}: $(t_{l_1}+t_3)/t_{p_i}$	Ratio of $(t_{l_1}+t_3)$ and pulse interval (t_{p_i})
F_{41}: f_{base}	Primary component frequency	F_{42}: $\lvert s_{base}\rvert$	Primary component magnitude
F_{43}: $f_{2^{nd}}$	2nd component frequency	F_{44}: $\lvert s_{2^{nd}}\rvert$	2nd component magnitude
F_{45}: $f_{3^{rd}}$	3nd component frequency	F_{46}: $\lvert s_{3^{rd}}\rvert$	2nd component magnitude

that detect feature dependencies using the concept of nearest neighbours that indirectly capture feature interactions [42].

3.5.3 FSCMRMR

The FSCMRMR algorithm finds an optimal set of mutually and maximally dissimilar features and can show the response variable effectively [15]. The method determines the redundancy and importance of variables based on their mutual information—pairwise mutual information of features and mutual information between a feature and the response. Instead of ranking single variables independently, this algorithm checks a balance between relevance (dependence between the features and the class) and redundancy (dependence among features) [43].

3.5.4 RFE

RFE selects those features in a training datasets which are most relevant in predicting the target by recursively eliminating a small number of features per loop. This in turn results in the elimination of collinearity in the model.

3.5.5 Ensemble feature selection

An ensemble feature selection method based on majority voting is applied to overcome the limitations of conventional feature selection methods [44]. In the beginning, a feature set consisting of 48 features from 218 recorded PPG is fed to an individual feature selection module (FSCMRMR, RLF, CFS, and RFE). Each module results in a set or subset of fea-

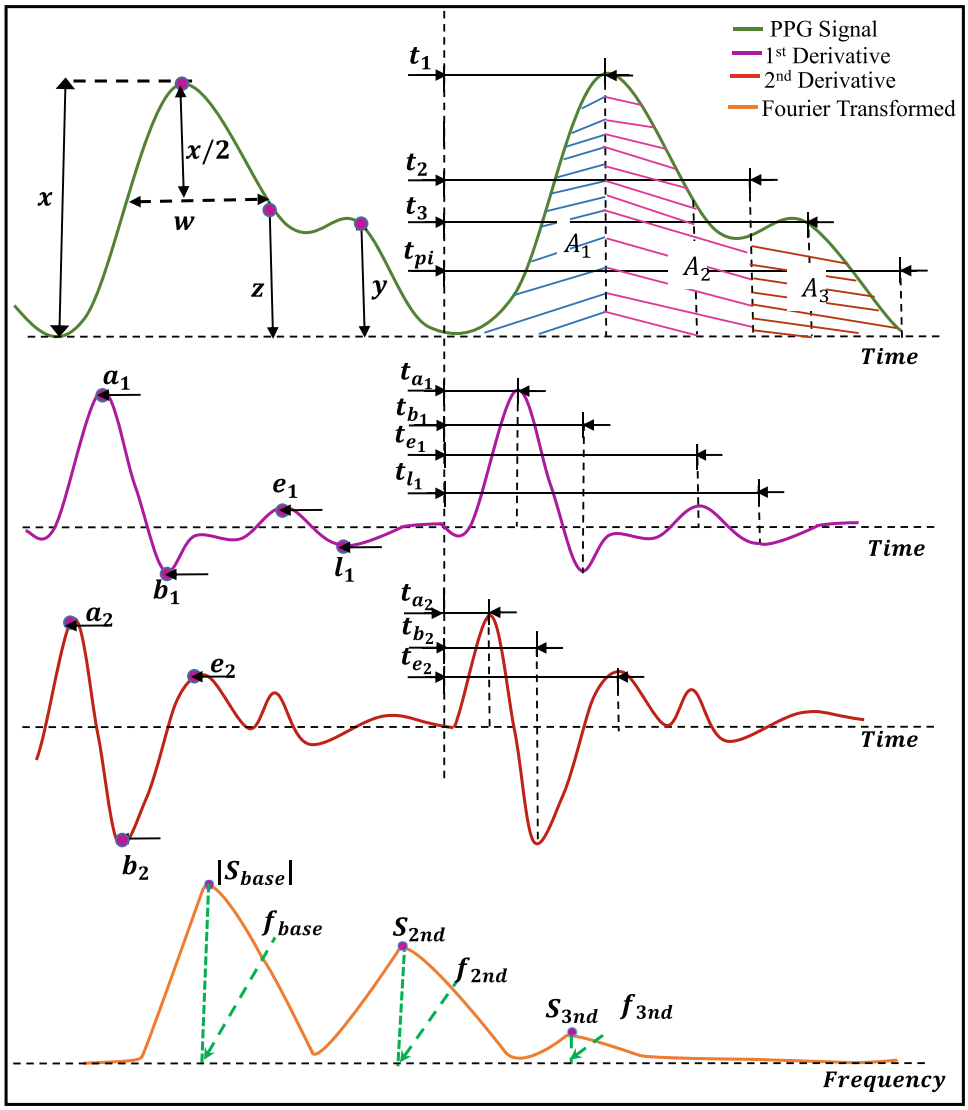

Fig. 8 Features extracted from PPG signal and its derivatives (VPPG and APPG) as well as Fourier Transformed PPG signal

tures for both the SBP and DBP estimations. If any feature selection module selected a feature, one vote was assigned to that feature. Then a voting score was assigned based on how many modules chose a feature. For example, if all modules selected feature F_1, its voting score will be four. The procedure of the ensemble feature selection approach is described in Algorithm 2.

3.6 Model construction

In this study, a feed-forward deep neural network is adopted to develop the BP estimation model on the basis of extracted features from PPG signals. It is equipped with weights, biases, and activation functions such as a rectified linear unit (ReLU) [45]. Figure 9 illustrates the architecture and training procedure for DNN based models. As demonstrated in Fig. 9, four hidden layers are used, where the first and third hidden layers contain 50 and 150 neurons, respectively. The second hidden layer consists of 100 neurons with a dropout unit of 0.25, while the fourth hidden layer consists of 200 neurons with a dropout unit of 0.50. The dropout method is a more efficient and alternative approach to dealing with DNN overfitting [46]. The output of each hidden layer processing unit can be represented as

$$BP_i = \sum_i \omega_i F_i + \beta \tag{11}$$

where F_i, β, and ω_i denote the input feature vectors, biases, and weights to the neuron, respectively. The hidden layer uses a nonlinear function to transform the input above as

$$\varphi_{Re}(BP) = \max(0, BP) \tag{12}$$

where φ_{Re} is the ReLU activation function. A linear activation function is applied to the output layer in the final state

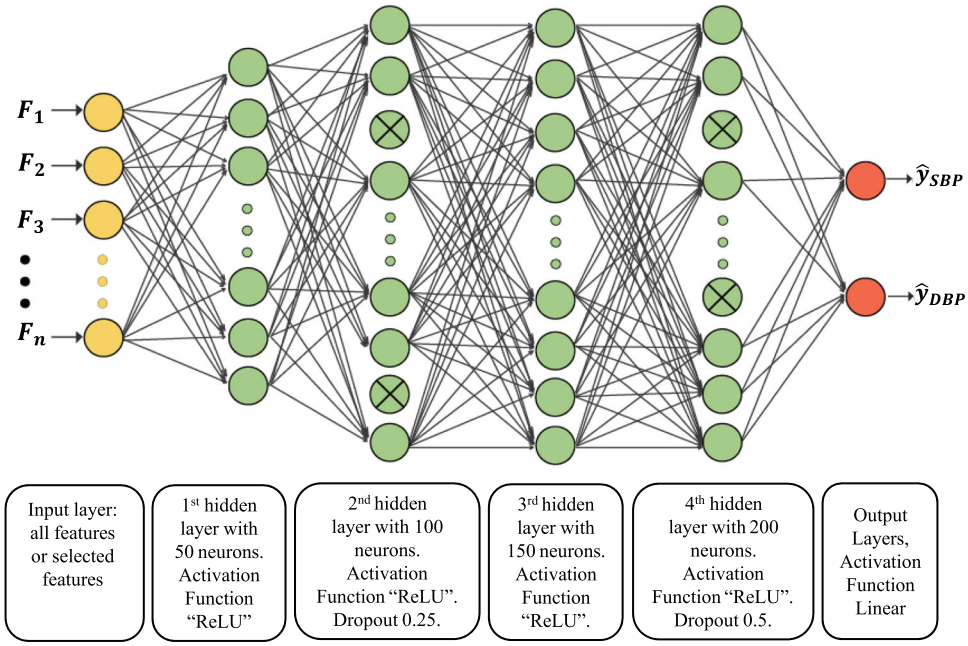

Fig. 9 The proposed architecture of DNN-based models for SBP and DBP estimation

Algorithm 1 PPG cycle detection and selection algorithm

Input: Series of continuous PPG signal S_{PPG}
Output: Best single PPG cycle B_{PPG}

$List_C \leftarrow \phi$;
/* $List_C \leftarrow$ list of valid cycle */
/* **Cycle Detection** */
while $time\_frame \geq 2.1$ **do**
  /* Duration of each PPG signal is 2.1s */
  Detect each cycle C_{PPG} **in** S_{PPG} **as follows:** ;
  Consider starting point (S_p), dicrotic notch (z), and ending point (E_p) are consecutive minima (M_a);
  Consider systolic peak (x) and diastolic peak (y) are consecutive maxima (M_x);
  Use $find\_peak$ from the NumPy module of python to detect the peaks of PPG signal and reduce the search time;
  /* Valid PPG cycle check (Fig. 7 (a)) */
  if C_{PPG} *contains* (M_a, M_x) **then**
    /* PPG cycle must have typical critical features like systolic peak, dicrotic notch, or diastolic peak (Fig. 1). */
    if x *is greater than* y, *and* z *is greater than* (S_p, E_p) **then**
      $List_C \leftarrow List_C \cup C_{PPG}$;
    else
      Discard C_{PPG};
  else
    Discard C_{PPG};
/* **Cycle Section** */
$B_{PPG} \leftarrow max_x(List_C)$ (Fig. 7 (b));
/* PPG cycle $List_C$ with the maximum systolic amplitude x */
return B_{PPG};

as

$$\varphi_{Li}(BP) = BP' \tag{13}$$

where $BP' = (-\infty, +\infty)$.

Algorithm 2 Ensemble feature selection technique

Input: $D = \{F_i, o_i\}_{i=1}^{m}$ $(F_i \in \mathbb{F}^T,\ o_i \in BP_a)$, BP_a = reference value, θ = threshold value for selecting the features, T = no. of features, K = no. of feature selection method
Output: Optimal feature set $List_V$

/* Initialization */
Set $\theta \leftarrow 2$, $List_V \leftarrow \phi$, $List F \leftarrow \phi$;
/* Calculate the optimal feature set using each feature selection algorithm */
$fsm \leftarrow \{cfs,\ relieff,\ fscmrmr,\ rfe\}$;
Calculate the optimal feature set using fsm;
for $t \leftarrow 1$ **to** T **do**
  for $k \leftarrow 1$ **to** K **do**
    if F_t *is selected by* fsm_k **then**
      $List F_t^{fsm_k} \leftarrow 1$;
    else
      $List F_t^{fsm_k} \leftarrow 0$;
/* Calculate voting score for each feature */
for $t \leftarrow 1$ **to** T **do**
  Calculate $V_{Score_t} \leftarrow \text{argmax}_{f_t \in F} \sum_{k=1}^{K} List F_t^{fsm_k}$;
  if $V_{Score_t} \geq \theta$ **then**
    $List_V \leftarrow List_V \cup F_t$;
Sort the $List_V$ according to V_{Score};
return $List_V$;

Table 4 Status of the hyperparameters used in our proposed DNN-based models

Hyperparameters	Status
Batch size	32
Learning rate α	0.01
Total hidden layers	4
Neurons count at 4 hidden layers	(50, 100, 150, 200)
Dropout at 2nd and 4th hidden layer	(0.25, 0.5)
Number of neurons at input layer	48 or selected features
Number of neurons at output layer	2
Activation function	ReLU, Linear
Optimizer	Adam

As a result, dense layer returns the sum of activation function. The proposed DNN models are trained on 100 epochs with respective batch size and learning rate of 32 and 0.01, respectively. Adam is utilized as the optimizer function to facilitate training processing and update the DNN parameters. Table 4 summarizes the hyperparameters employed in the proposed DNN-based models. These proposed models for BP estimation are trained and tested using all features and selected features.

3.7 Performance measurement parameters

The overall performance of our proposed BP measuring method is evaluated in accordance with the mean difference (ME), standard deviation (STD), mean absolute percentage error (MAPE), mean square error (MSE), root mean square error (RMSE), and the coefficient of determination (R^2). The formulas are as follows:

$$ME = \frac{1}{n}\sum_{n}(BP_e - BP_a) \tag{14}$$

$$STD = \sqrt{\frac{\sum_n (BP_e - BP_a - ME)^2}{n-1}} \tag{15}$$

$$MAPE = \frac{1}{n}\sum_{n}\left|\frac{BP_a - BP_e}{BP_a}\right| * 100 \tag{16}$$

$$MSE = \frac{1}{n}\sum_{n}(BP_a - BP_e)^2 \tag{17}$$

$$RMSE = \sqrt{MSE} \tag{18}$$

$$MAE = \frac{1}{n}\sum_{n}|BP_a - BP_e| \tag{19}$$

$$R^2 = 1 - \frac{\sum_n (BP_a - BP_e)^2}{\sum_n (BP_a - \overline{BP})^2} \tag{20}$$

where $\overline{BP} = \frac{1}{n}\sum_n BP_a$, and BP_a is the reference value while BP_e is the estimated value.

4 Result and discussion

4.1 Feature selection

Table 5 demonstrates the outcomes of several features selection techniques. Using feature selection algorithms, features are ranked according to their significance. Both CFS and ReliefF reduced the features from 48 to 16 for SBP, respectively. Similarly, CFS and ReliefF selected only 16 and 17 features, respectively, for DBP. Then, the remaining two FS methods (FSCMRMR and RFE) selected only 5 and 6 features for SBP, whereas 6 and 9 features for DBP, respectively.

Table 6 portraits the voting score of individual features using the ensemble approach (Algorithm 2). In this study, as four different FS methods are applied to the extracted feature set, selecting a feature at least has to have a voting score of two. For both SBP and DBP estimations, it is evident from

Table 5 The selected features from different feature selection algorithms

Dataset	Feature selection technique	Selected features	Count
SBP	CFS	F_{47}, F_{14}, F_{12}, F_{28}, F_{25}, F_{29}, F_{26}, F_2, F_4, F_6,F_3, F_{45}, F_{40}, F_{48}, F_{41}, F_{43}	16
	ReliefF	F_{47}, F_{16}, F_{14}, F_{27}, F_{28}, F_2, F_1, F_{25}, F_{44}, F_8, F_3, F_5, F_6, F_7, F_{42}, F_{48}	16
	FSCMRMR	F_{47}, F_{19}, F_{23}, F_{45}, F_{41}	5
	RFE	F_{47}, F_{45}, F_{25}, F_{26}, F_4, F_{28}	6
DBP	CFS	F_{47}, F_{14}, F_{12}, F_{26}, F_{25}, F_{29}, F_{28}, F_2, F_4, F_1, F_3, F_6, F_{40}, F_{41}, F_{48}, F_{43}, F_{45}	17
	ReliefF	F_{47}, F_{16}, F_{14}, F_{27}, F_{26}, F_2, F_1, F_{25}, F_{44}, F_8, F_3, F_5, F_6, F_7, F_{42}, F_{48}	16
	FSCMRMR	F_{47}, F_{27}, F_{22}, F_3, F_{45}, F_{41}	6
	RFE	F_{45}, F_{12}, F_{14}, F_4, F_{47}, F_{41}, F_{40}, F_{25}, F_{28}	9

* Note: Features are sorted according to their importance with corresponding feature selection algorithm

Table 6 Voting scores of the corresponding features in the proposed ensemble feature selection approach

Feature	SBP	Feature	DBP
	Voting score		Voting score
F_{47}	4	F_{47}	4
F_{28}	3	F_{45}	3
F_{25}	3	F_{25}	3
F_{45}	3	F_{14}	3
F_{14}	2	F_{3}	3
F_{26}	2	F_{41}	3
F_{2}	2	F_{6}	2
F_{4}	2	F_{12}	2
F_{6}	2	F_{26}	2
F_{3}	2	F_{40}	2
F_{41}	2	F_{27}	2
F_{48}	2	F_{28}	2
–	–	F_{4}	2
–	–	F_{1}	2
–	–	F_{2}	2
–	–	F_{48}	2

Table 6 that all the four FS methods voted for features F_{47}. Similarly, features F_{28}, F_{25}, and F_{45} have a voting score of three for SBP and features F_{45}, F_{25}, F_{14}, F_{3}, and F_{41} for DBP, respectively. The rest of the features in Table 6 are voted by the two FS methods for both SBP and DBP.

4.2 Robustness performance of models

We used DNN-based models to estimate the SBP and DBP using all features and selected features. A 10-fold cross-validation method was used to divide the data into training and testing sets. It is also noted that each recorded signal of the PPG-BP database has its unique ID. Our study used it to prevent overlapping the subjects of the training set and the testing set.

In the beginning, the proposed DNN-based models are trained and validated using all features for BP value estimation. The DNN models are validated using a 10-fold cross-validation approach, where each fold contains reference and estimated BP values. The mean performances of the models are then calculated following that. Table 7 summarizes the overall performance of the proposed ensemble feature selection method and existing feature selection methods along with our proposed DNN-based models. The estimated accuracies of DNN models using all features are $R^2 = 0.867$ and MAE = 3.631 mmHg for SBP, 0.805 and 2.387 mmHg for DBP, respectively.

Features selection is crucial to minimize the probability of models getting overfit. Due to this, four feature selection algorithms existing in the literature (CFS, ReleifF, FSCMRMR, and RFE) are used individually for selecting relevant feature subsets. Finally, the selected features from the individual FS method are fed to the DNN models. Among these four FS algorithms, CFS along with the DNN model provided better results of $R^2 = 0.952$ and MAE = 2.804 mmHg for SBP and ReliefF with $R^2 = 0.936$ and MAE = 1.796 mmHg for DBP, respectively.

Furthermore, the proposed ensemble feature selection technique is applied to select the best optimal feature set that provided best results when combining with DNN models for the estimation of BP values. According to obtained result in Table 7, this approach provides the highest estimated accuracy of $R^2 = 0.962$ and MAE = 2.480 mmHg for SBP and 0.955 and 1.499 mmHg for DBP, respectively. Figure 10 shows the accuracy (R^2-score) respective to various feature selection techniques along with the number of selected features for SBP and DBP, where our proposed ensemble feature selection technique performs better than others.

Figure 11 demonstrates a histogram of estimated errors for BP values. It is evident from both the histograms that the error values for BP estimation are distributed normally around zero. The elemental cause beneath the greater appearance of the estimated error of SBP compared to those of the

Table 7 Performance comparison using various existing feature selection methods and our proposed ensemble feature selection method along with the DNN models

Selection criteria	SBP					DBP				
	R^2	MAE	MSE	RMSE	MAPE	R^2	MAE	MSE	RMSE	MAPE
All features	0.867	3.631	47.925	6.923	3.057	0.805	2.387	24.572	4.957	3.786
CFS	0.952	2.804	18.652	4.318	3.224	0.933	1.773	7.381	2.716	3.042
ReliefF	0.941	3.191	20.704	4.550	3.137	0.936	1.796	7.817	2.795	3.029
FSCMRMR	0.913	3.149	27.966	5.288	3.187	0.908	1.923	10.471	3.235	2.955
RFE	0.946	3.020	19.300	4.393	3.120	0.907	2.233	12.217	3.495	2.986
Proposed method	**0.962**	**2.480**	**13.760**	**3.709**	**3.187**	**0.955**	**1.499**	4.869	2.206	2.721

Bold indicates the best performing model

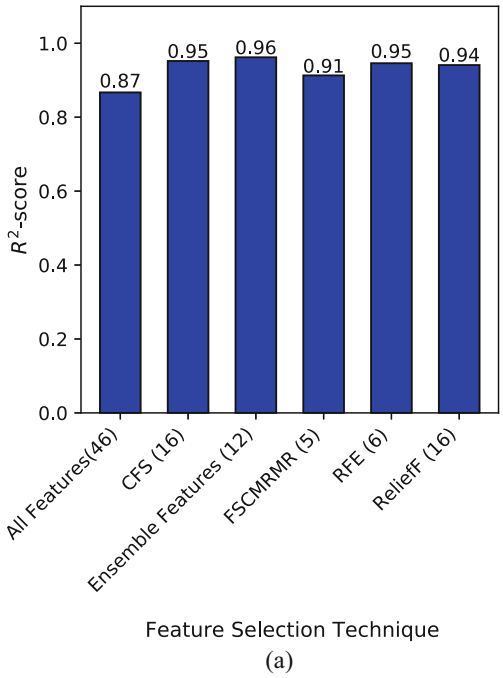

(a)

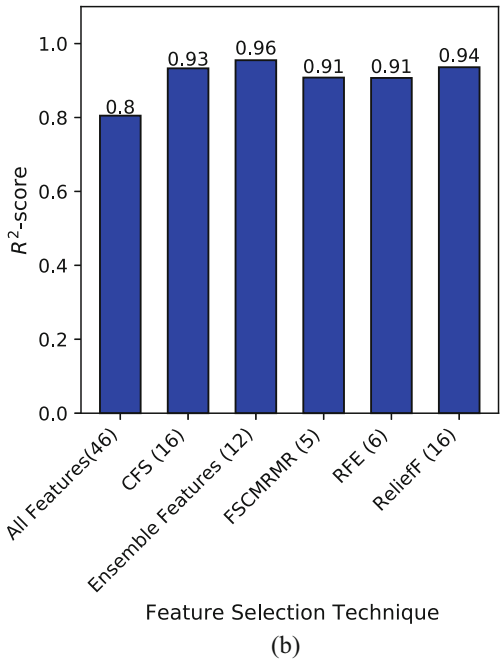

(b)

Fig. 10 Accuracy (R^2-score) Vs feature selection methods: **a** SBP and **b** DBP

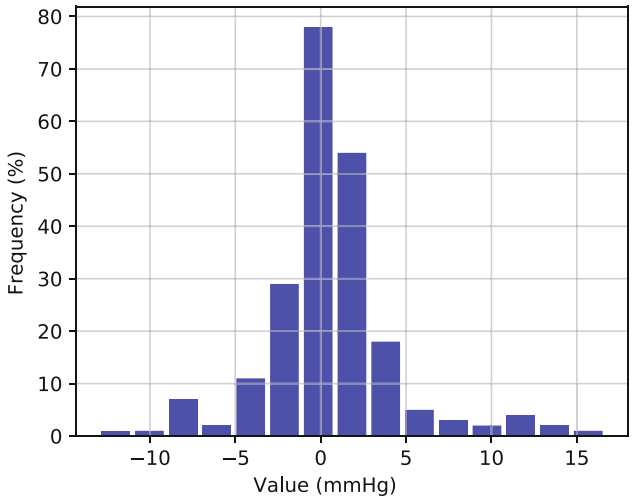

(a)

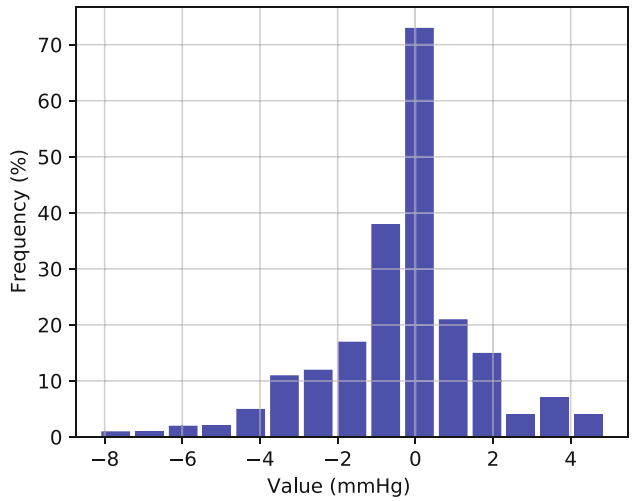

(b)

Fig. 11 Histograms of estimated errors in DNN-based models: **a** SBP and **b** DBP

DBP ones is the dispersion of SBP target values being nearly twice as large as the dispersion of DBP target values.

Figure 12a and c presents a correlation-based comparison of the estimated values with the reference BP values. Furthermore, the Bland–Altman plot is depicted in Fig. 12b and d for evaluating the distance of the estimated value from the reference one. Bland-Altman defines the agreement between the reference value and the estimated value by establishing limits of agreement. It can be concluded from the plots that a higher percentage of estimated values are within the limits of agreement ($md \pm 1.96 * sd$). The limits of agreement for SBP with hybrid selected features at a 95% confidence interval were $\{-7.87$ mmHg and 6.98 mmHg$\}$ and for DBP were $\{-4.88$ mmHg and 4.68 mmHg$\}$. However, samples having extremely high or low BP values are not approximated as accurate as other samples. The main reason of this issue is the presence of fewer subjects with extremely high or low BP within the training set, which restricts the model performance in anticipating continuous BP values.

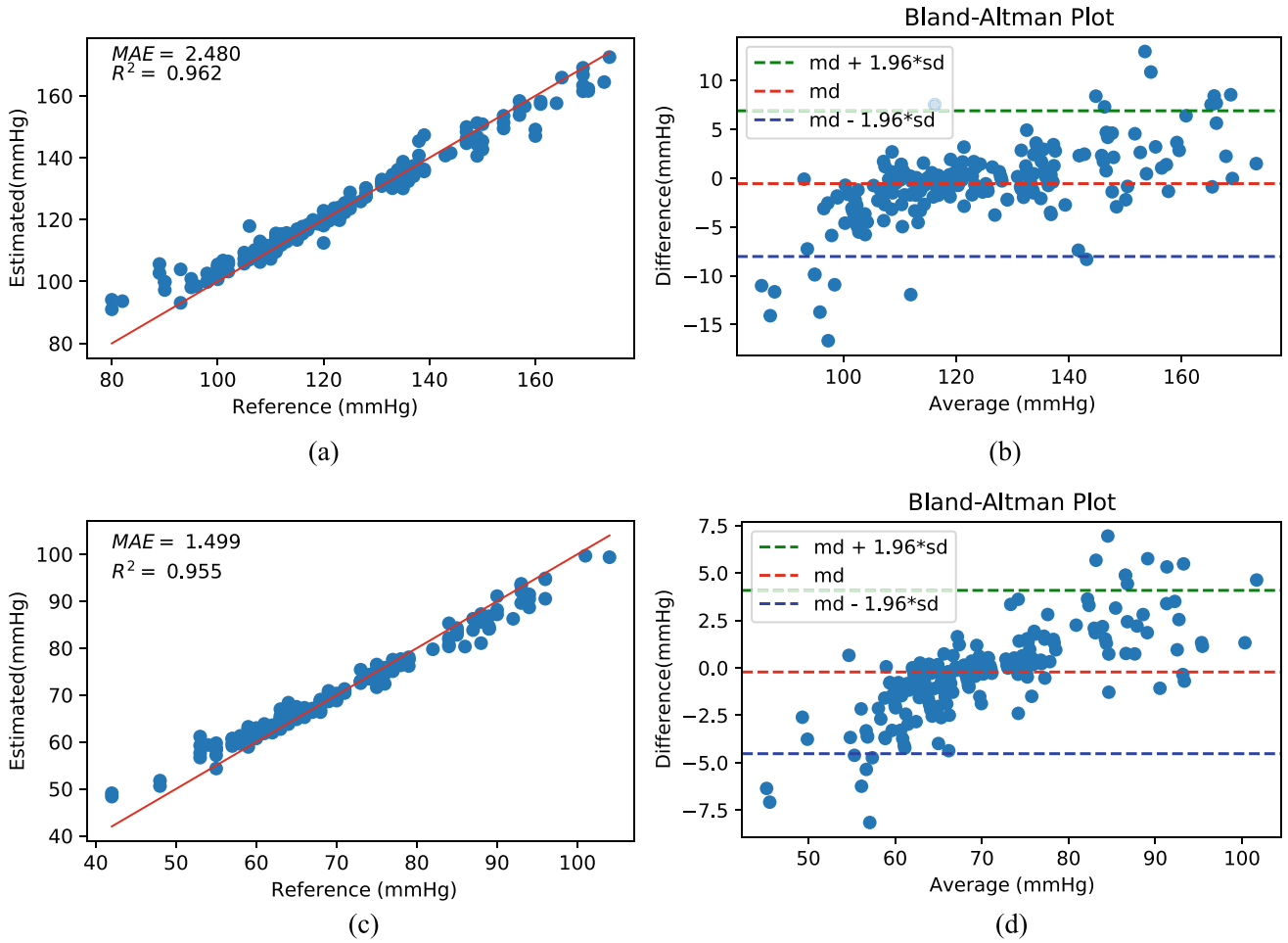

Fig. 12 Correlation and agreement (Bland-Altman) plots of SBP and DBP with reference values at testing stage for DNN model based on hybrid feature selection: **a** relationship (SBP), **b** agreement (SBP), **c** relationship (DBP), and **d** agreement (DBP)

4.3 Evaluation using the AAMI standard

A comparison between the results of BP estimation using our proposed method and the Advancement of Medical Instrumentation (AAMI) criterion is depicted in Table 8. According to the specification of the AAMI, the mean and standard deviation must not be greater than 5 mmHg and 8 mmHg, respectively, for BP measuring devices. In addition to this criteria, this protocol directs that the number of participants should be at least 85 to ensure the equipment or method's accuracy. Table 8 shows that our proposed method has mean values that are significantly less than the maximum allowable mean value. In terms of the STD criterion, both SBP and DBP have STD values within the 8 mmHg standard margin.

Table 8 Comparison of this paper results with AAMI

		ME (mmHg)	STD (mmHg)	Subjects
AAMI [47]	BP	≤ 5	≤ 8	≥ 85
Our results	SBP	−0.471	4.105	125
	DBP	−0.049	2.194	125

Table 9 Comparison of this paper results with BHS

		Cumulative error percentage		
		$\leq$ 5mmHg	$\leq$ 10mmHg	$\leq$ 15mmHg
Our results	SBP	91%	95%	99%
	DBP	96%	99%	100%
BHS [48]	Grade A	60%	85%	95%
	Grade B	50%	75%	90%
	Grade A	40%	65%	85%

Table 10 Comparison of our proposed method with several existing methods that only used PPG signal

Work	Dataset	Method	Performance ($MAE \pm STD$) mmHg	
			SBP	DBP
Kachuee et al. [8]	MIMIC II	AdaBoost	11.2 ± 10.1	5.35 ± 6.14
Gaurav et al. [24]	MIMIC II	ANN	4.47 ± 6.85	3.21 ± 4.72
Zhang and Feng [16]	Univ. of Queensland	SVM	11.64 ± 8.22	7.61 ± 6.78
Mousavi et al. [25]	MIMIC II	AdaBoost	3.97 ± 7.99	2.43 ± 3.37
Hasanzadeh et al. [14]	MIMIC II	AdaBoost	8.22 ± 1.38	4.17 ± 4.22
Panwar et al. [17]	MIMIC II	LRCN	3.97 ± 0.06	2.30 ± 0.19
Chowdhury [15]	PPG-BP	GPR	3.02 ± 9.29	1.74 ± 5.54
Li and Laleg-Kirati [21]	MIMIC II	FFNN	7.44 ± 7.37	5.09 ± 5.66
Maqsood et al. [22]	PPG-BP	GRU	3.68 ± 4.28	5.34 ± 5.24
Proposed	**PPG-BP**	**DNN**	$\mathbf{2.48 \pm 4.10}$	$\mathbf{1.49 \pm 2.19}$

Bold indicates the best performing model

4.4 Evaluation using the BHS standard

An illustration for the evaluation of our proposed method according to the British Hypertension Society (BHS) grading criteria is shown in Table 9. BHS grades the BP monitoring devices according to their percentage of cumulative errors underneath three different threshold values, i.e., 5, 10, and 15 mmHg [48]. In accordance with the BHS standard, the performance of our method is persistent, with grade A for both SBP and DBP estimations.

4.5 Comparison with other works

Table 10 presents the comparative analysis of the proposed methodology with the contemporary works to validate the effectiveness of our proposed methodology. From the comparison, it can be seen that our proposed method achieved an average $MAE \pm STD$ of 2.48 ± 4.105 mmHg for SBP and 1.49 ± 2.194 mmHg for DBP estimation which are better compared to the existing methods. It is clear from these results that our proposed methodology can be used in real-time healthcare applications.

Table 10 summarizes previous studies that have estimated the BP using only the PPG signal but have assessed their methodologies using a variety of datasets. Since these research works used different datasets and/or a small number of patients than the proposed approach, it is difficult to make a precise comparison for BP estimation. Furthermore, PPG-BP is a new dataset, and only a few studies have been conducted utilizing this dataset so far. The studies by [15, 22] used the PPG-BG dataset, whereas our proposed technique performed better than these studies.

5 Conclusion

In this paper, we proposed a BP monitoring approach by combining ensemble feature selection technique with deep neural network. Primarily, the proposed methodology consists of signal acquisition, signal filtration, baseline correction, and feature extraction. An ensemble feature selection technique is applied to obtain the most promising feature set based on major voting by four feature selection algorithms. Then, DNN based models are developed, and a 10-fold cross-validation method is applied to validate the models. The combination of the ensemble feature selection method and DNN models provides the best accuracy for estimating continuous blood pressure. The accuracy of our proposed BP estimation method is validated using the AAMI and BHS standards. According to the BHS, our proposed method has grade A for both SBP and DBP estimations. The findings reveal that this approach to BP estimation could be applicable for clinical applications. In the future, we plan to extend our work by including the other physiological parameters such as blood component levels and oxygen saturation (SpO2) as well as computing the whole process automatically in cloud server and sending the result to the smartphone user.

Acknowledgements This work is supported in part by Khulna University of Engineering & Technology.

Author Contributions S. M. Taslim Uddin Raju: conceptualization, methodology, writing—original draft. Safin Ahmed Dipto: conceptualization, methodology, writing—review and editing. Md Imran Hossain: visualization, investigation. Md. Abu Shahid Chowdhury: formal analysis, visualization, writing—original draft. Fabliha Haque: writing—review and editing, project administration. Ayesha Tun Nashrah: investigation, validation. Araf Nishan: writing—review and editing,

visualization. Mahamudul Hasan Khan: writing—review and editing, revision. M. M. A. Hashem: supervision.

Declarations

Conflict of Interest The authors declare no Conflict of interest.

Ethics Approval and Consent to Participate Not applicable.

Consent for Publication Not applicable.

References

1. Wu C-Y et al (2015) High blood pressure and all-cause and cardiovascular disease mortalities in community-dwelling older adults. Medicine 94(47)
2. Ma HT (2014) A blood pressure monitoring method for stroke management. BioMed Research International 2014
3. Ding X-R et al (2016) Continuous blood pressure measurement from invasive to unobtrusive: celebration of 200th birth anniversary of Carl Ludwig. IEEE J Biomed Health Inform 20(6):1455–1465
4. Tao K-m, Sokha S, Yuan H-b (2019) Sphygmomanometer for invasive blood pressure monitoring in a medical mission. Anesthesiology 130(2):312–312
5. Chandrasekhar A et al (2018) Smartphone-based blood pressure monitoring via the oscillometric finger-pressing method. Sci Transl Med 10(431):eaap8674
6. van Geene W (1993) Clinical evaluation of a blood pressure controller in anaesthesia
7. Chakraborty A, Goswami D, Mukhopadhyay J, Chakrabarti S (2020) Measurement of arterial blood pressure through single-site acquisition of photoplethysmograph signal. IEEE Trans Instrum Meas 70:1–10
8. Kachuee M, Kiani MM, Mohammadzade H, Shabany M (2016) Cuffless blood pressure estimation algorithms for continuous health-care monitoring. IEEE Trans Biomed Eng 64(4):859–869
9. Haque MR, Raju SMTU, Golap MA-U, Hashem MMA (2021) A novel technique for non-invasive measurement of human blood component levels from fingertip video using DNN based models. IEEE Access 9:19025–19042
10. Sun Y, Thakor N (2015) Photoplethysmography revisited: from contact to noncontact, from point to imaging. IEEE Trans Biomed Eng 63(3):463–477
11. Castaneda D, Esparza A, Ghamari M, Soltanpur C, Nazeran H (2018) A review on wearable photoplethysmography sensors and their potential future applications in health care. Int J Biosens Bioelectron 4(4):195
12. Jarchi D, Casson AJ (2017) Towards photoplethysmography-based estimation of instantaneous heart rate during physical activity. IEEE Trans Biomed Eng 64(9):2042–2053
13. Sinchai S, Kainan P, Wardkein P, Koseeyaporn J (2018) A photoplethysmographic signal isolated from an additive motion artifact by frequency translation. IEEE Trans Biomed Circ Syst 12(4):904–917
14. Hasanzadeh N, Ahmadi MM, Mohammadzade H (2019) Blood pressure estimation using photoplethysmogram signal and its morphological features. IEEE Sensors J 20(8):4300–4310
15. Chowdhury MH et al (2020) Estimating blood pressure from the photoplethysmogram signal and demographic features using machine learning techniques. Sensors 20(11):3127
16. Zhang Y, Feng Z (2017) A SVM method for continuous blood pressure estimation from a PPG signal. In: Proceedings of the 9th international conference on machine learning and computing, pp 128–132
17. Panwar M, Gautam A, Biswas D, Acharyya A (2020) PP-Net: a deep learning framework for PPG-based blood pressure and heart rate estimation. IEEE Sensors J 20(17):10000–10011
18. Samimi H, Dajani HR (2022) Cuffless blood pressure estimation using calibrated cardiovascular dynamics in the photoplethysmogram. Bioengineering 9(9):446
19. Mukkamala R et al (2015) Toward ubiquitous blood pressure monitoring via pulse transit time: theory and practice. IEEE Trans Biomed Eng 62(8):1879–1901
20. Teng X, Zhang Y (2003) Continuous and noninvasive estimation of arterial blood pressure using a photoplethysmographic approach. In: Proceedings of the 25th annual international conference of the ieee engineering in medicine and biology society (IEEE Cat. No. 03CH37439), vol 4, pp 3153–3156. IEEE
21. Li P, Laleg-Kirati T-M (2021) Central blood pressure estimation from distal PPG measurement using semiclassical signal analysis features. IEEE Access 9:44963–44973
22. Maqsood S, Xu S, Springer M, Mohawesh R (2021) A benchmark study of machine learning for analysis of signal feature extraction techniques for blood pressure estimation using photoplethysmography (PPG). IEEE Access 9:138817–138833
23. El-Hajj C, Kyriacou PA (2021) Cuffless blood pressure estimation from PPG signals and its derivatives using deep learning models. Biomed Signal Process Control 70:102984
24. Gaurav A, Maheedhar M, Tiwari VN, Narayanan R (2016) Cuff-less PPG based continuous blood pressure monitoring—a smartphone based approach. In: 2016 38th annual international conference of the IEEE engineering in medicine and biology society (EMBC), pp 607–610. IEEE
25. Mousavi SS, Firouzmand M, Charmi M, Hemmati M, Moghadam M, Ghorbani Y (2019) Blood pressure estimation from appropriate and inappropriate PPG signals using a whole-based method. Biomed Signal Process Control 47:196–206
26. Peter L, Noury N, Cerny M (2014) A review of methods for non-invasive and continuous blood pressure monitoring: pulse transit time method is promising? Irbm 35(5):271–282
27. Mukkamala R, Hahn J-O (2017) Toward ubiquitous blood pressure monitoring via pulse transit time: predictions on maximum calibration period and acceptable error limits. IEEE Trans Biomed Eng 65(6):1410–1420
28. Möbius P, Remoissenet, M (1997) Waves called solitons. concepts and experiments. berlin etc., springer-verlag 1996. xx, 260 pp., dm 78, 00. isbn 3-540-60502-9. Zeitschrift Angewandte Mathematik und Mechanik 77(7):560–560
29. Ding X-R, Zhang Y-T, Liu J, Dai W-X, Tsang HK (2015) Continuous cuffless blood pressure estimation using pulse transit time and photoplethysmogram intensity ratio. IEEE Trans Biomed Eng 63(5):964–972
30. Zheng Y-L, Yan BP, Zhang Y-T, Poon CC (2014) An armband wearable device for overnight and cuff-less blood pressure measurement. IEEE Trans Biomed Eng 61(7):2179–2186
31. Westerhof N, Lankhaar J-W, Westerhof BE (2009) The arterial windkessel. Med Biol Eng Comput 47(2):131–141
32. Miao F et al (2017) A novel continuous blood pressure estimation approach based on data mining techniques. IEEE J Biomed Health Inform 21(6):1730–1740
33. Liang Y, Chen Z, Elgendi M (2021) PPG-BP database. 2018. https://figshare.com/articles/dataset/PPG-BP_Database_zip/5459299. Accessed 06 April 2021
34. Liang Y, Elgendi M, Chen Z, Ward R (2018) An optimal filter for short photoplethysmogram signals. Sci data 5(1):1–12

35. Elgendi M (2012) On the analysis of fingertip photoplethysmogram signals. Curr Cardiol Rev 8(1):14–25
36. Chatterjee A, Roy UK (2018) PPG based heart rate algorithm improvement with Butterworth IIR Filter and Savitzky-Golay FIR Filter. In: 2018 2nd International conference on electronics, materials engineering & nano-technology (IEMENTech), pp 1–6. IEEE
37. Holschneider M, Kronland-Martinet R, Morlet J, Tchamitchian P (1990) A real-time algorithm for signal analysis with the help of the wavelet transform. In: Wavelets, pp 286–297. Springer
38. Xing X, Sun M (2016) Optical blood pressure estimation with photoplethysmography and FFT-based neural networks. Biomed Opt Express 7(8):3007–3020
39. Zahoor U (2011) Baseline wandering removal from human electrocardiogram signal using projection pursuit gradient ascent algorithm. Int J Electr Comput Sci IlECS/IJENS 9(9):11–13
40. Kavsaoğlu AR, Polat K, Hariharan M (2015) Non-invasive prediction of hemoglobin level using machine learning techniques with the PPG signal's characteristics features. Appl Soft Comput 37:983–991
41. Kira K et al (1992) The feature selection problem: traditional methods and a new algorithm. Aaai 2:129–134
42. Urbanowicz RJ, Meeker M, La Cava W, Olson RS, Moore JH (2018) Relief-based feature selection: introduction and review. J Biomed Inform 85:189–203
43. Acid S, De Campos LM, Fernández M (2011) Minimum redundancy maximum relevancy versus score-based methods for learning Markov boundaries. In: 2011 11th International conference on intelligent systems design and applications, pp 619–623. IEEE
44. Singh BK, Verma K, Thoke A, Suri JS (2017) Risk stratification of 2d ultrasound-based breast lesions using hybrid feature selection in machine learning paradigm. Measurement 105:146–157
45. Aggarwal CC (2018) Training deep neural networks. In: Neural networks and deep learning, pp 105–167. Springer
46. Srivastava N, Hinton G, Krizhevsky A, Sutskever I, Salakhutdinov R (2014) Dropout: a simple way to prevent neural networks from overfitting. J Mach Learn Res 15(1):1929–1958
47. for the Advancement of Medical Instrumentation A et al (1987) American national standards for electronic or automated sphygmomanometers. ANSI/AAMI SP 10-1987
48. O'brien E, Waeber B, Parati G, Staessen J, Myers MG (2001) Blood pressure measuring devices: recommendations of the European Society of Hypertension. Bmj 322(7285):531–536

S. M. Taslim Uddin Raju was born on February 19, 1996 in Feni, Bangladesh. He has received his M.Sc. and B.Sc. degree in Computer Science and Engineering (CSE) from the Khulna University of Engineering & Technology (KUET), Khulna, Bangladesh in 2019 and 2022 respectively. He is also working as a Lecturer with the CSE Department, KUET. His research interests are in bioinformatics, health informatics, biomedical engineering, deep learning, machine learning, natural language processing, and image processing. He has published some conference papers and journals in these domains. He is also working on some articles about these topics with his students and colleagues.

Safin Ahmed Dipto was born in Dhaka, Bangladesh, in 1999. He is currently an undergraduate student in the Dept. of Computer Science and Engineering (CSE) at Khulna University of Engineering Technology (KUET). His research interests are in machine learning, deep learning, biomedical engineering, bioinformatics, and image processing.

Md Imran Hossain was born in Comilla, Bangladesh, in 1998. He is currently an undergraduate student in the Dept. of Computer Science and Engineering (CSE) at Khulna University of Engineering & Technology (KUET). His research interests are in machine learning, deep learning, biomedical engineering, bioinformatics, and image processing.

Md Abu Shahid Chowdhury is currently working as a Lecturer in the Department of Biomedical Engineering, Khulna University of Engineering & Technology (KUET), Khulna-9203, Bangladesh. He has completed his BSc in Biomedical Engineering from this University in 2019 and started working as a lecturer in this university on December 17, 2120. Parallelly with his job, he is pursuing MSc in Biomedical Engineering from this University. He is very much interested in Biosensor, Biomedical Signal Processing, Biomedical Image Processing, Bio-nanotechnology, Biomaterials, Human Machine Interface. His ambition is to utilize his competence in building a strong career in the research field related to Biomedical Engineering.

Fabliha Haque was born on March 20, 1997. She has persuaded her B.Sc. degree in Computer Science and Engineering (CSE) from Khulna University of Engineering & Technology (KUET), Khulna, Bangladesh. Her research interests include Machine Learning, Deep Learning, Natural Language Processing and Biomedical Engineering.

Ayesha Tun Nashrah was born in Dhaka, Bangladesh, is currently pursuing her B.Sc. degree in Biomedical Engineering from Khulna University of Engineering & Technology (KUET), Khulna, Bangladesh. Her research interests include biomedical instrumentation, cell and molecular engineering, tissue engineering, drug delivery, biomaterials and machine learning.

Araf Nishan was born in Dhaka, Bangladesh. He has persuaded his B.Sc. engineering degree in Computer Science and Engineering at Khulna University of Engineering & Technology, Khulna, Bangladesh. His research interests include Bioinformatics, Biomedical Engineering, Health Informatics, Biomedical Instrumentation, Computer Vision, Image Processing, Natural Language Processing, Machine Learning, Deep Learning, GANs, Deep Reinforcement Learning and Artificial Intelligence.

Md Mahamudul Hasan Khan was born in Mymensingh, Dhaka, Bangladesh, in 1990. He received the M.Sc. degree in Computer Science from Mercy University in 2023. Moreover, he also received B.Sc. degree in Computer Science and Engineering from Khulna University of Engineering & technology (KUET) in 2013. He is now currently working as ITS 2 programmer in NYS Office of Information Technology Services, USA and also looking for opportunity to pursuit PhD. Degree in Machine learning and Data Science. His research interests are in bioinformatics, health informatics, biomedical engineering, deep learning, machine learning, data science and image processing. His two papers are under review in journals. He is also working in some projects with his colleagues for future publication.

M. M. A. Hashem received the Bachelors degree in Electrical and Electronic Engineering from Khulna University of Engineering & Technology (KUET), Khulna, Bangladesh in 1988, Masters degree in Computer Science from Asian Institute of Technology (AIT), Bangkok, Thailand in 1993 and PhD degree in Artificial Intelligence Systems from the Saga University, Japan in 1999. He is currently a Professor in the Dept. of Computer Science and Engineering, Khulna University of Engineering & Technology (KUET), Bangladesh. His research interests include Artificial Intelligence, Machine Learning, Bioinformatics, Biomedical Engineering, Health Informatics, Biomedical Instrumentation, Evolutionary Computations, Soft Computing, etc. He has published more than 100 referred articles in international Journals/Conferences. He is a co-author of a book titled Evolutionary Computations: New Algorithms and their Applications to Evolutionary Robots, Series: Studies in Fuzziness and Soft Computing, Vol. 147, Springer-Verlag, Berlin/New York, ISBN: 3-540-20901-8, (2004).

Authors and Affiliations

S. M. Taslim Uddin Raju[1] · Safin Ahmed Dipto[1] · Md Imran Hossain[1] · Md. Abu Shahid Chowdhury[2] · Fabliha Haque[1] · Ayesha Tun Nashrah[2] · Araf Nishan[3] · Md Mahamudul Hasan Khan[1] · M. M. A. Hashem[1]

Safin Ahmed Dipto
ahmmed1707024@stud.kuet.ac.bd

Md Imran Hossain
hossain1707072@stud.kuet.ac.bd

Md. Abu Shahid Chowdhury
shahid@bme.kuet.ac.bd

Fabliha Haque
fablihahaque13@gmail.com

Ayesha Tun Nashrah
nashrah1715016@stud.kuet.ac.bd

Araf Nishan
mahmud.nishan@hotmail.com

Md Mahamudul Hasan Khan
shuvomahamud@gmail.com

M. M. A. Hashem
hashem@cse.kuet.ac.bd

1 Department of Computer Science and Engineering, Khulna University of Engineering & Technology, Khulna 9203, Bangladesh

2 Department of Biomedical Engineering, Khulna University of Engineering & Technology, Khulna 9203, Bangladesh

3 Department of Business Administration, International American University, Los Angeles, CA 90010, USA